FLOW IN A ROTATING CAVITY WITH A PERIPHERAL INLET AND OUTLET OF COOLING AIR

X Gan, I Mirzaee, J M Owen, D A S Rees and M Wilson
School of Mechanical Engineering
University of Bath,
Bath, UK

ABSTRACT

In some engines, corotating−gas−turbine discs are cooled by air introduced at the periphery of the system. The air enters through holes in a stationary peripheral casing and leaves through the rim seals between the casing and the discs. This paper describes a combined computational and experimental study of such a system for a range of flowrates and for rotational Reynolds numbers of up to Re_ϕ = 1.5 x 10^6. Computations are made using an axisymmetric elliptic solver, incorporating the Launder−Sharma low−Reynolds−number k−ε turbulence model, and velocity measurements are obtained using laser−Doppler anemometry.

The stationary peripheral casing creates a recirculation region: there is radial outflow in boundary layers on the discs and inflow in the core between the boundary layers. The radial extent of the recirculation region increases as the flow rate increases and as the rotational speed decreases. In the core, the radial and tangential components of velocity, V_r and V_ϕ, are invariant in the axial direction, and the measured values of V_ϕ conform to a Rankine−vortex flow. The agreement between the computed and measured velocities is not as good as that found for other rotating−disc systems, and deficiencies in the turbulence model are believed to be responsible.

NOMENCLATURE

a, b	inner, outer radius of disc
A, B	constants in equation 1.6
c	inlet swirl ratio
c_{eff}	effective swirl ratio
C_w	nondimensional mass flow rate (=m/μb)
G	gap ratio (=s/b)
k	turbulent kinetic energy
m	mass flow rate
r	radial coordinate
Re_ϕ	rotational Reynolds number (=ρΩb^2/μ)
s	axial gap between discs
U_τ	friction velocity (=√(τ_w/ρ))
V_r,V_ϕ,V_z	time−averaged velocities in r,ϕ,z directions
x	nondimensional radius (=r/b)
x_e	radial location of end of source region
x_1	radial location of stagnation point (where V_ϕ = Ωr)
y	distance normal to wall
y^+	wall−distance Reynolds number (=ρU_τy/μ)
z	axial coordinate measured from disc 1
ε	turbulent energy dissipation rate
λ_T	turbulent flow parameter (=$C_w Re_\phi^{-0.8}$)
μ	dynamic viscosity
ρ	density
ϕ	tangential coordinate
τ_w	total wall shear stress
Ω	angular speed of discs

1 INTRODUCTION

The flow and heat transfer associated with air−cooled gas−turbine discs can be modelled using simple rotating−disc systems (see Owen and Rogers 1989, 1995). Fig 1 shows schematic diagrams of three such systems, referred to as rotating cavities, which are used to represent corotating turbine or compressor discs. Fig 1a, the rotating cavity with a radial outflow of cooling air, represents the usual case for turbine−disc cooling systems. Fig 1b, the rotating cavity with a radial inflow of cooling air, is used to simulate the case where air is extracted between two compressor discs. Fig 1c, the rotating cavity with a peripheral flow of cooling air, is used to model a novel method of cooling corotating turbine discs. Whereas the flow structure for the first two cases has been studied extensively (see, for

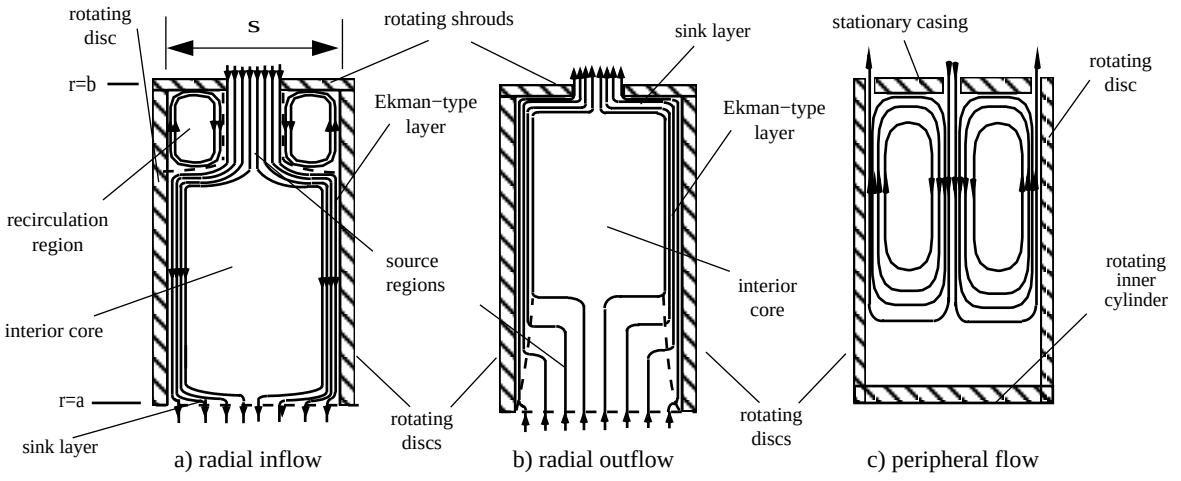

Fig. 1 Schematic diagram of rotating cavities

example, Owen and Pincombe 1980, Chew, Owen and Pincombe 1984, Owen, Pincombe and Rogers 1985, Firouzian et al 1985, 1986, Farthing and Owen 1991, Owen and Rogers 1995), little is known about the peripheral−flow case.

For the radial−inflow case shown in Fig 1a, air enters the cavity through holes in the "shroud" (or rotating cylindrical casing) at a radius of r = b (or x = 1, where x = r/b) with a mass flow rate m (m < 0, by convention, for radial inflow) and an inlet swirl ratio c (where $c = V_\phi/\Omega b$, V_ϕ being the tangential component of velocity of the air). In the source region, where viscous effects are small, the angular momentum of the fluid is conserved and a free vortex is formed such that

$$rV_\phi = c\Omega b^2 \qquad (1.1)$$

or

$$V_\phi/\Omega r = cx^{-2} \qquad (1.2)$$

The air in the source region is progressively entrained into the boundary layers on the discs. If c < 1, the flow in the boundary layers is radially outward when $V_\phi/\Omega r < 1$, and is radially inward when $V_\phi/\Omega r > 1$. The radius at which $V_\phi = \Omega r$ represents a stagnation "point", above which the flow recirculates as shown in Fig 1a. This recirculation creates mixing between the radially outward flow in the boundary layer and the radially inward flow of air entering the cavity, and the conservation of angular momentum results in the effective swirl ratio c_{eff} being greater than the inlet swirl ratio c. Under these conditions, equation (1.2) becomes

$$V_\phi/\Omega r = c_{eff}x^{-2} \qquad (1.3)$$

and the nondimensional stagnation radius x_1 is given by

$$x_1 = c_{eff}^{1/2} \qquad (1.4)$$

For $x < x_1$ the flow in the boundary layer is radially inward, and the edge of source region, at $x = x_e$, the point where all air entering the system has been entrained into the boundary layers; and the radial extent of the source region increases with increasing flowrate and with decreasing rotational speed. For $x < x_e$, nonentraining Ekman−type layers are formed on each disc between which the interior core rotates at a speed greater than the discs. Under isothermal conditions, when there is symmetry about the mid−plane (z = ½s), the radial and axial components of velocity, V_r and V_z, are zero in the core and V_ϕ is invariant with z. The air leaves the system at r=a via the so−called sink layer.

For radial outflow (where m > 0), the locations of the source and sink are reversed, as shown in Fig 1b, and unless $V_\phi/\Omega r > 1$ at r = a, there is no recirculation in the source region. The flow in the Ekman−type layers and the interior core is similar to that for inflow, although, for the outflow case, the flow is radially outward in the layers, the core rotates at a speed slower than the discs, and the air leaves the system, via the sink layer, through holes in the rotating shroud.

For the peripheral−flow case, Fig 1c, the air enters the system through holes in a stationary casing at r = b and leaves through the clearances between this casing and the discs. The cavity is sealed at r = a by a rotating inner cylinder attached to both discs. The fact that the shroud is stationary and the flow enters and leaves at r = b makes the peripheral−flow case different from the other two.

For the radial−inflow and outflow cases, when m = 0, solid−body rotation occurs creating a forced vortex where

$$V_\phi = \Omega r \qquad (1.5)$$

For the peripheral flow case, when m = 0, the stationary casing creates recirculation in the cavity in which fluid moves radially outwards in boundary layers on the discs and radially inward in the interior core between the boundary layers. This creates a so−called Rankine vortex (see Owen and Rogers 1995), in which

$$V_\phi/\Omega r = Ax^{-2} + B \qquad (1.6)$$

where A and B are invariant with x. It is shown below that this structure occurs even when $m \neq 0$.

It is the purpose of this paper to describe a combined computational and experimental investigation of the rotating cavity with a peripheral flow of cooling air, and to compare the computed distributions of the axial and tangential components of velocity with measured values for a range of flowrates and rotational speeds. The experimental apparatus and computational method are described in Sections 2 and 3, respectively, and the computed and measured results are discussed in Section 4. Conclusions are presented in Section 5.

2 EXPERIMENTAL APPARATUS AND INSTRUMENTATION

2.1 Experimental rig

Fig 2 shows a diagram of the rotating−cavity rig used in this study. The discs were 762 mm in diameter, one of which was made from steel and the other from transparent polycarbonate providing optical access for laser−Doppler−anemometry (LDA) measurements. The discs were spaced 113 mm apart (G = 0.30) and a cylinder of 382−mm diameter, made from Rohacell (a lightweight foam material), was clamped between the two discs to provide an impermeable boundary at a/b = 0.50. The whole assembly could be rotated at speeds up to 1500 rev/min by a 15kW thyristor−controlled d.c. motor.

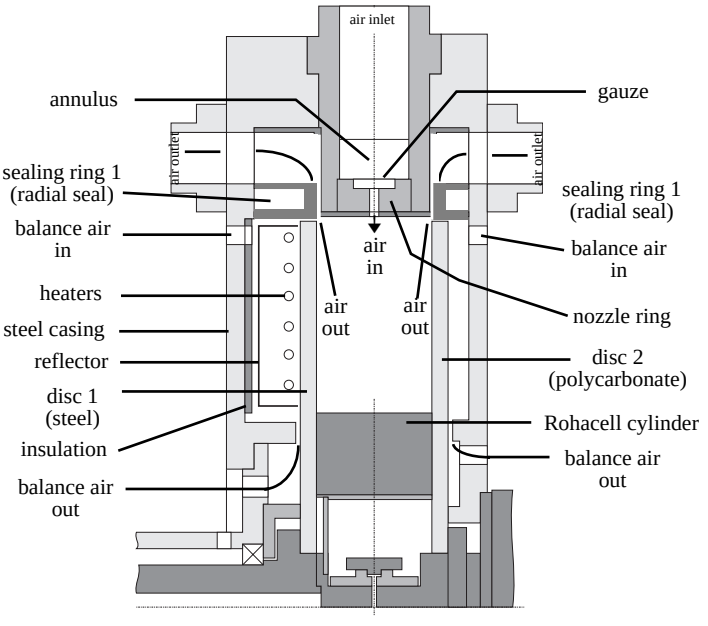

Fig. 2 Rotating cavity rig

Air could be admitted to the periphery of the cavity via a stationary steel nozzle ring containing 38 equi−spaced nozzles of 11.3 mm diameter, with the axis of each nozzle in the mid−plane (z/s = ½) on a radial line through the axis of rotation. The nozzle ring was housed in a steel casing which contained seals that were used to control the flow of air out of the system. The seal clearances were 1mm, and by balancing the air pressure on either side of each seal it was possible to control the ratio of the flowrates from the left−hand and right−hand seals (seals 1 and 2). For the experiments discussed below, each outlet flowrate was made equal to half the inlet flowrate: the difference between the inlet flowrate and the sum of the outlets was less than 6% of the inlet value.

The surrounding stationary casing contained a window, made from transparent polycarbonate, to provide optical access for the LDA measurements. The inlet air was supplied from a Bellis and Morecombe compressor, capable of producing 0.5 kg/s at an absolute pressure of 5 bar. Although the casing could be pressurised and the steel disc could be heated, the tests described below were conducted at conditions close to atmospheric pressure and temperature.

It should be pointed out that the inner surface of the nozzle ring was covered with Rohacell foam, which creates an effective adiabatic surface for heat−transfer tests. This foam, which formed the cylindrical boundaries at r = a and r = b, had an average roughness of 30 μm. (Tests conducted after those reported here suggest that the Rohacell surfaces may not be "aerodynamically smooth".)

2.2 Instrumentation

The rotational speed was measured, with an uncertainty of ±1 rev/min, by means of a 60−pole timing disc, a transducer and a frequency counter.

The flowrates were measured, with an uncertainty of ±3%, using orifice plates manufactured in accordance with British Standards BS1042 and installed in the inlet and outlet pipes connected to the stationary casing.

The LDA measurements were made using a back−scatter optical system, Bragg−cell frequency shift and a single−channel IFA−750 burst correlator manufactured by TSI. The laser was Spectra−Physics Model 164−A, a nominal 4W argon−ion laser which produced up to 800 mW on the green line (514.5mm); for the tests described here, up to 400 mW was used. The light from the laser was transmitted to the optics via an optical−fibre cable with an efficiency of around 60%. The optics were mounted on a traversing table with the optical axis parallel to the axis of rotation of the cavity. This enabled either the radial or the tangential components (V_r or V_ϕ) to be measured at any one time. The computer−controlled table was traversed automatically, and measurements were made at a number of radial and axial locations inside the rotating cavity.

The processor could measure Doppler frequencies up to 90 Mhz for signal−to−noise ratios as low as −5dB. The beam spacing was 50 mm, and a converging lens with a focal length of 250 mm was used to produce an optical probe volume of 1.4 mm length and 0.14 mm waist diameter. The measurements of V_ϕ were checked by positioning the probe volume inside the polycarbonate disc: the measured velocities were within 1% of the disc speed. For measurements in the core outside the boundary layers on the discs, on−axis measurements of V_ϕ could be made. For V_r, and for V_ϕ inside the boundary layers where flare from the surfaces was a problem, off−axis measurements were necessary; this restricted the field−of−view. The positional uncertainty of the location of the probe volume was 0.13 mm, and it was possible to obtain measurements as close as 0.5 mm to the polycarbonate disc and 1.5 mm to the steel one. The uncertainty in the velocity measurements was estimated as ±3%.

The inlet air was seeded with micron−sized oil particles from a TSI particle generator. For the measurements made with no superposed flow, the inlet air was turned off after the cavity had been charged with particles. The size of the particles was small enough to make the "radial migration error", due to the centrifuging action of the rotating air, an insignificant quantity.

2.3 Range of test parameters

The main nondimensional variables of relevance to this problem are the gap ratio, G, the radius ratio, a/b, the nondimensional flowrate, C_w, the rotational Reynolds number, Re_ϕ , and the turbulent flow parameter, λ_T (where $\lambda_T = C_w Re_\phi^{-0.8}$). In particular, the magnitude of λ_T has a strong effect on the flow structure for a rotating cavity with a radial inflow or outflow (see Owen and Rogers 1995); it is shown in Section 4 that λ_T also has a strong effect on the flow structure for the peripheral−flow case.

In gas turbines, values of Re_ϕ are usually of the order of 10^7 whereas the maximum value for the rig is around 1.5×10^6. In disc−cooling systems in engines, the magnitude of C_w is also much higher than that used on the rig. However, for the tests described below, $0 \le |\lambda_T| \le 0.1$, which is typical of the range used for disc cooling in engines, and the resulting flow structure is believed to be representative of that at high values of Re_ϕ. The values of G and a/b (0.3 and 0.5 respectively) are also representative of the engine geometry modelled.

3 Computational method

Incompressible flow computations were carried out using an axisymmetric finite−volume solver for the discretised forms of the steady−flow, Reynolds−averaged, Navier−Stokes and energy equations, using staggered storage locations for radial and tangential velocity components in a cylindrical−polar grid (details of the equations solved are given by Wilson et al (1995)). The turbulent fluxes were calculated using the low−Reynolds−number k−ε turbulence model due to Launder and Sharma (1974). The convergence of the SIMPLEC pressure−correction procedure for the coupled conservation equations was accelerated using a fixed V−cycle, Full Approximation Storage multigrid algorithm, as described by Vaughan et al (1989) for a solver from which the present code was developed.

The computational grid was generated by matching near−wall and interior zones in both the axial and radial directions using geometric expansions away from solid surfaces, and also a geometric contraction toward the radial mid−plane between the discs for superposed flow calculations. The expansion factors varied between 1.0 and 1.22, and the grid−points near each solid surface were located so that $y^+ < 0.5$, ensuring that the turbulence equations were implemented as required into the laminar sub−layer of the boundary layers attached to the discs and shrouds. Sealed−system computations were carried out on a 91 x 131 (radial x axial) grid, the solutions being virtually unchanged when a 67 x 67 grid was used. For cases with superposed flow, a 91 x 91 grid was used, without further grid−dependence tests, as illustrated in Fig 3. The symmetry about the mid−plane of the present flow problem was not exploited, in view of a number of other computations also being carried out on the same configuration (but not reported here) where different boundary conditions dictate solutions that are not symmetric.

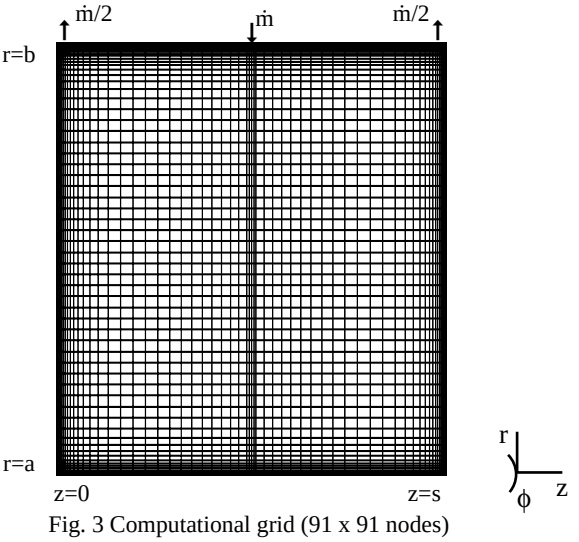

Fig. 3 Computational grid (91 x 91 nodes)

The inlet nozzles were modelled as an equivalent−area annular slot in the mid−plane of the stationary outer casing. The outlet boundaries were axial clearances between the tip of each disc and the outer casing, which matched the clearances in the experimental rig. The following boundary conditions were used:

i) no−slip velocity conditions at solid surfaces;

ii) uniform distributions for the radial component of velocity, Vr, at inlet and outlet (deduced from a prescribed mass flowrate matching the experimental conditions), with zero axial velocity, Vz, at inlet and outlet (prescribing mass flow−rates at the two axial clearances enforced the test condition of equal division of the flow between these outlets: in other cases being studied, the division of the flow is not equal but again taken directly from experimental measurements);

iii) zero swirl at inlet ($V_\phi = 0$) and derivative conditions for the tangential component of velocity at the outlets ($\partial V_\phi / \partial r = 0$).

Convergence of the iterative method was monitored by means of the total absolute residual for each of the dependent variables . The aggregrate continuity error was normalised either by the superposed mass flowrate or, for a sealed system with no superposed flow, by the mass flowrate circulating at a fixed radial location. The residuals for the other variables were normalised by the product of this mass flowrate and characteristic values of the variables. The characteristic value for k was taken as $k = 10^{-2}\Omega b^2$, with ε then determined by assuming a turbulence Reynolds number of 100. The normalised total residuals were less than 10^{-3} for all variables for the results reported here, and the root−mean−square change in each variable between iterations was less than 2×10^{-5} by this stage.

4 COMPUTED AND MEASURED RESULTS

4.1 Computed streamlines

Figs 4 and 5 show the computed "streamlines" in the r − z plane for rotational Reynolds numbers of Re_ϕ = 3.75 x 10^5 and 1.5 x 10^6 respectively. For each figure, computations are presented for nondimensional flowrates of C_w = 0, −1500 and −3000, where the negative sign is used by convention to denote that the inlet flow is radially inward: the values of λ_T for each case are also shown on the figures.

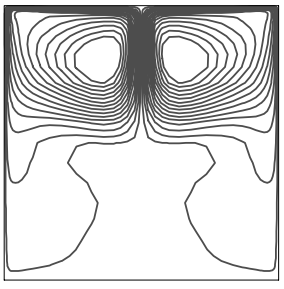

a) C_w=0.0 (λ_T = 0.0)

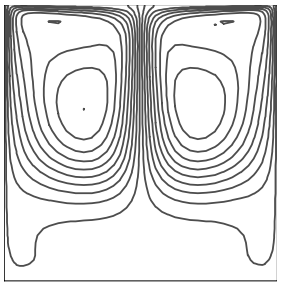

b) C_w = -1500 (λ_T = -0.052)

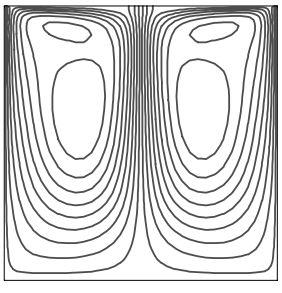

c) C_w = -3000 (λ_T = -0.104)

Fig. 4 Computed streamlines for Re_ϕ = 3.75 x 10^5

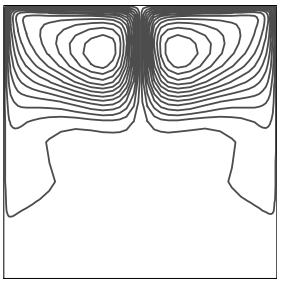

a) C_w = 0.0 (λ_T = 0.0)

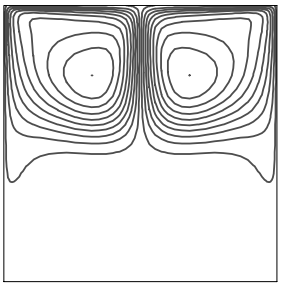

b) C_w = -1500 (λ_T = -0.0172)

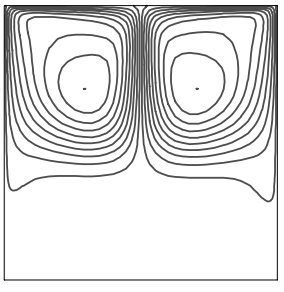

c) C_w = -3000 (λ_T = -0.034)

Fig. 5 Computed streamlines for Re_ϕ = 1.5 x 10^6

Referring to Fig 4, the following observations can be made. The basic flow structure for all cases comprises two counter−rotating circulation regions, symmetrical about the mid−plane (z/s = ½). Air enters, through the slot in the mid−plane at r = b, and flows radially inward before being entrained into the boundary layers on the rotating discs. Fluid in these boundary layers moves radially outwards and, at r = b, some leaves the system and the rest moves axially from the discs to the mid−plane in boundary layers on the stationary casing. Although the air enters the cavity at r = b without swirl (c = 0), it is shown below that the mixing between the fluid entering and that recirculating imparts swirl to the incoming air such that $V_\phi > 0$ for r < b; this process is similar to that described above for the source region in the radial inflow case.

Fig 4a shows that, even when C_w = 0, the shear on the stationary casing creates a powerful recirculation region: if the casing were rotating at the same speed as the discs, there would be solid−body rotation with no recirculation. Figs 4b and 4c show that, as expected, the size (or radial extent) of the recirculation region increases as $|C_w|$ increases, and for C_w = −3000 recirculation occurs throughout the cavity.

Figs 5a, b, c show similar characteristics to those described above although, for this higher value of Re_ϕ, the size of the source region is smaller, as is the case for the rotating cavity with a radial inflow or outflow of fluid described in Section 1. Inspection of Figs 4 and 5 show that, as for the rotating cavity with a radial inflow, the size of the recirculation region increases as $|\lambda_T|$ increases. Streamlines computed at other values of λ_T are consistent with this trend. Comparisons between the computed and measured velocities are discussed below.

4.2 Computed and measured velocities

Fig 6 shows the axial distribution of the radial and tangential components of velocity at x = 0.55, 0.75 and 0.85 for λ_T = 0, −0.034 and −0.104.

In Fig 6a, for λ_T = 0, the computed and measured values of $V_r/\Omega r$ show characteristics consistent with those described above for the streamlines: there is a radial inflow in the core and radial outflow in thin boundary layers on the rotating discs; as explained in Section 2.2, it was not possible to obtain LDA measurements close to the steel disc, at z/s = 0. The agreement between the computed and measured values of $V_\phi/\Omega r$ at x = 0.85 are better for λ_T = −0.034 than for λ_T = 0; no measurements are available for the other values of x in Fig 6b.

Fig 6c, for λ_T = −0.104, shows broadly similar results, but the agreement between the computations and measurements is worse for $V_r/\Omega r$ than for $V_\phi/\Omega r$; in the latter case, the agreement is good. Both the computed and the measured velocities in Fig 6 indicate that the radial inflow, and hence the recirculation in the cavity, increases as $|\lambda_T|$ increases. Results obtained at other values of λ_T are consistent with those presented here.

Fig 7 shows the computed and measured radial variation of $V_\phi/\Omega r$ in the mid−plane for the values of λ_T used in Fig 6. For all cases, $V_\phi/\Omega r$ increases as x decreases. For λ_T = 0 and −0.034, the computations overestimate the measured velocities for x > 0.6; for λ_T = −0.104, the agreement is much better.

Fig 8 shows the velocities in Fig 7 plotted against x^{-2} rather than x. In all cases, the experimental data conform almost perfectly to the classical Rankine vortex given by equation (1.6). It should be pointed out that $x^{-2} < 1$ is outside the physical domain.

The value of B in equation (1.6) is given by the value of $V_\phi/\Omega r$ at x^{-2} = 0: B decreases as $|\lambda_T|$ increases indicating, not surprisingly, that the flow tends to a free vortex as the magnitude of the flowrate

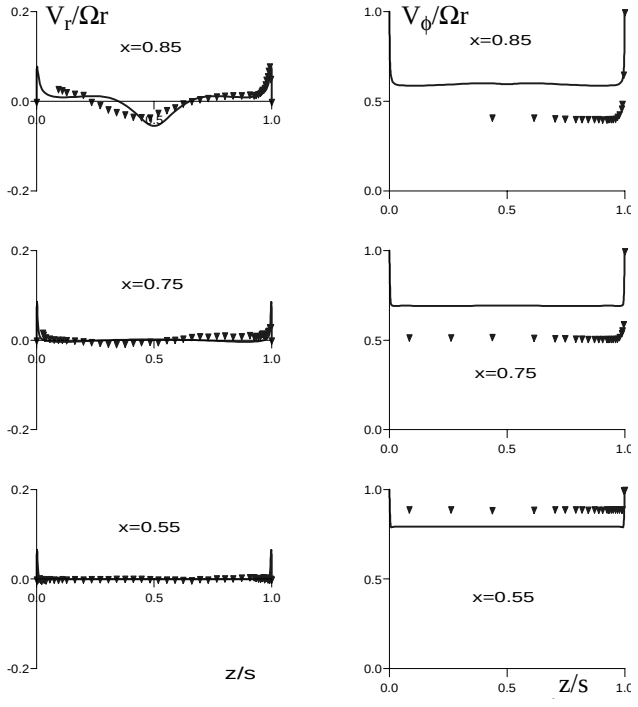

Fig. 6a Comparison between computed and measured variation of $V_r/\Omega r$ and $V_\phi/\Omega r$ with z/s for

$C_W = 0$, $Re_\phi = 1.5 \times 10^6$ ($\lambda_T = 0.0$)

▼ measurements —— computations

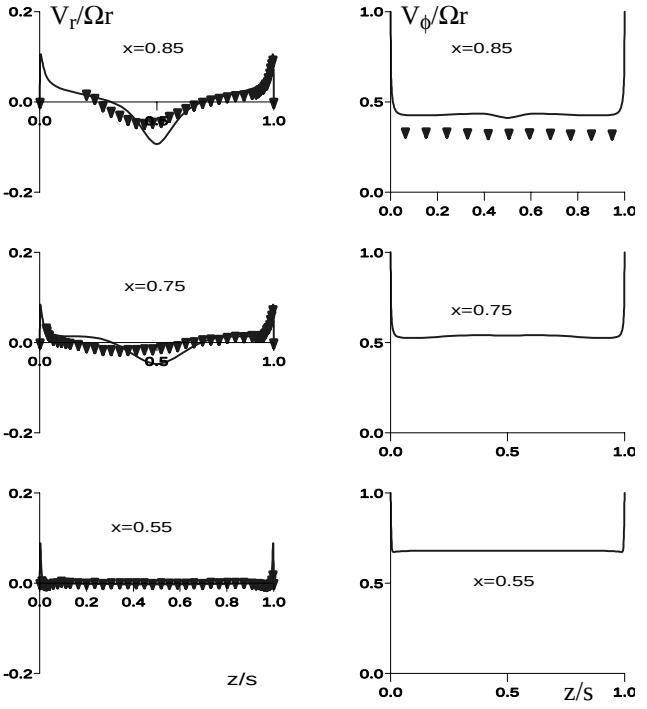

Fig. 6b Comparison between computed and measured variation of $V_r/\Omega r$ and $V_\phi/\Omega r$ with z/s for

$C_W = -3000$, $Re_\phi = 1.5 \times 10^6$ ($\lambda_T = -0.034$)

▼ measurements —— computations

is increased. Again, results obtained at other values of λ_T are consistent with those presented here.

Another point of interest in Fig 8 is the value of $V_\phi/\Omega r$ at x = 1: this corresponds to the effective swirl ratio, c_{eff}, discussed in Section 1. Although the inlet swirl ratio, c, is zero, the exchange of angular momentum in the mixing region near the stationary casing adds swirl to the incoming air. The approximate value of c_{eff}, based on the Rankine−vortex line at $x^{-2} = 1$, reduces from 0.3 at $\lambda_T = 0$ to 0.1 at $\lambda_T = -0.104$. This reduction of ceff with increasing $|\lambda_T|$ also occurs in a rotating cavity with a radial inflow, again illustrating the similarity of these two flows.

The agreement between the computed and measured velocities shown in Fig 8 is unsatisfactory, but it improves as $|\lambda_T|$ increases. The computations fail to produce the Rankine−vortex flow in the core; this is disappointing if not completely surprising. The authors have investigated many possible reasons for the relatively poor agreement between these computations and measurements including physical effects and computational deficiencies. Effects considered include: roughness on the inner and outer cylindrical surfaces of the experimental rig (see Section 2.1); possible ingress of external fluid through the seals in the rig; modelling deficiencies caused by representing discrete holes in the nozzle ring of the rig by a circular slot in the computations; inadequacy of the turbulence model. Although these investigations are still proceeding, it appears to be the last effect that is the most significant, and there are encouraging signs that relatively simple, Richardson number−based modifications to the ε equation in the Launder−Sharma model can produce improved agreement between the computed and measured results. As well as investigating such modifications, the authors are continuing their study of the peripheral−flow problem. Future work, which will be reported elsewhere, will include the use of alternative geometries and the measurement of heat transfer, together with the testing of non−linear eddy viscosity models of turbulence.

5 CONCLUSIONS

A combined computational and experimental study bas been conducted for a rotating cavity with a peripheral inflow and outflow of air. Results are presented for G = 0.3, a/b = 0.5, $Re_\phi = 3.75 \times 10^5$ and 1.5×10^6 , and $0 \le |\lambda_T| \le 0.1$. The following observations can be made:

- the stationary peripheral casing creates a recirculation region in the cavity with two counter−rotating vortices in the r − z plane symmetrical about the mid−plane (z/s = ½). Fluid flows radially inward in the core and radially outward in the boundary layers on the rotating discs.

- The size of the recirculation region increases as $|\lambda_T|$ increases.

- Although the air enters the cavity with an inlet swirl ratio, c, of zero, mixing with the recirculating air increases the swirl of the radial inflow such that the effective swirl ratio, c_{eff}, is greater than zero; c_{eff} decreases as $|\lambda_T|$ increases.

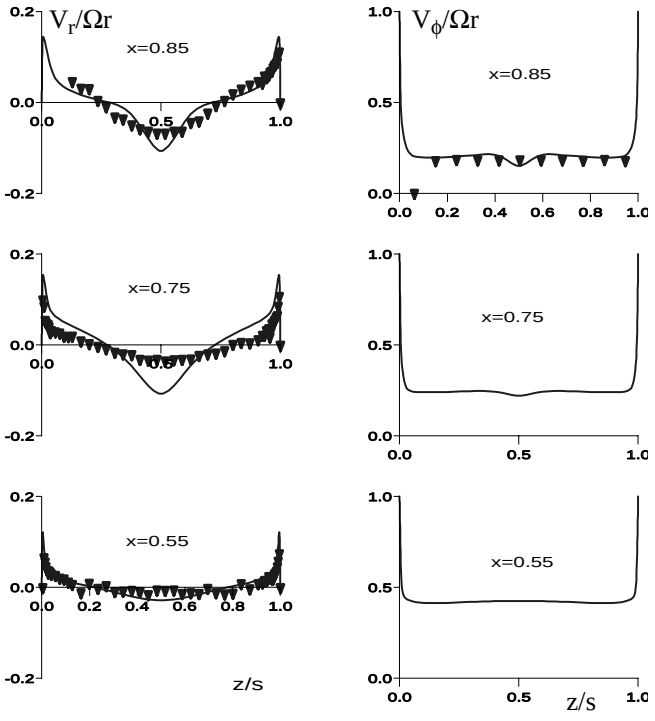

Fig. 6c Comparison between computed and measured variation of $V_r/\Omega r$ and $V_\phi/\Omega r$ with z/s for

$C_W = -3000$, $Re_\phi = 3.75 \times 10^5$ ($\lambda_T = -0.104$)

▼ measurements —— computations

- The radial and tangential components of velocity, V_r and V_ϕ, are invariant with z in the core, and the measured values of V_ϕ conform to a Rankine vortex, where $V_\phi/\Omega r = Ax^{-2} + B$; B decreases (that is, the flow tends to a free vortex) as $|\lambda_T|$ increases.

- Agreement between the computed and measured values of V_ϕ improves as $|\lambda_T|$ increases; the converse is true for V_r .

- Although the reasons for the disappointing agreement between some of the computed and measured velocities are not fully understood, deficiencies in the low−Reynolds−number k−ε turbulence model are believed to be the principal cause.

ACKNOWLEDGEMENTS

The authors wish to thank BMW−Rolls−Royce GmbH for funding the experimental programme and the Defence Research Agency and the Engineering and Physical Sciences Research Council, UK, for funding the computational work.

REFERENCES

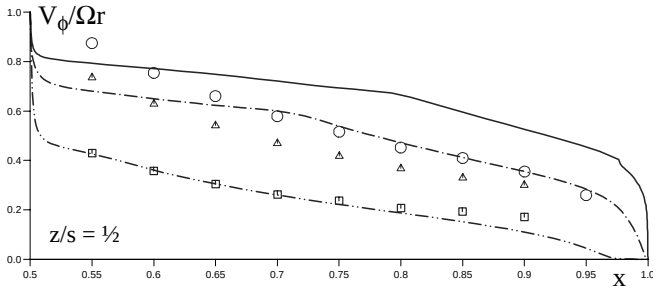

Fig. 7 Comparison between computed and measured variation of $V_\phi/\Omega r$ with x in the mid−plane (key as Fig. 8 below)

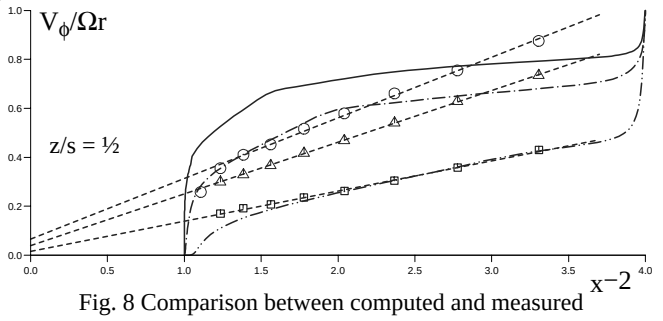

Fig. 8 Comparison between computed and measured variation of $V_\phi/\Omega r$ with x^{-2} in the mid−plane

C_w	Re_ϕ	λ_T	measurments	computations
0	1.5×10^6	0	○	——
-3000	1.5×10^6	-0.034	△	—·—·
-3000	3.75×10^5	-0.104	□	—··—

Rankine vortex lines

Farthing, P.R. and Owen, J.M. 1991, De−swirled radial inflow in a rotating cavity. Int. J. Heat and Fluid Flow, 12, 63−70

Firouzian, M.O., Owen, J.M., Pincombe, J.R. and Rogers, R.H. 1985, Flow and heat transfer in a rotating cylindrical cavity with a radial inflow of fluid. Part 1: The flow structure. Int. J. Heat and Fluid Flow, 6, 228−234

Firouzian, M.O., Owen, J.M., Pincombe, J.R. and Rogers, R.H. 1986, Flow and heat transfer in a rotating cylindrical cavity with a radial inflow of fluid. Part 2: Velocity, pressure and heat transfer measurements. Int. J. Heat and Fluid Flow, 7, 21−27

Launder, B. E. and Sharma, B. I. 1974, Application of the energy dissipation model of turbulence to flow near a spinning disc, Letters in Heat and Mass Transfer, 1, 131−138

Owen, J.M. and Pincombe, J.R. 1980, Velocity measurements inside a rotating cylindrical cavity with a radial outflow of fluid. J. Fluid Mech., 99, 111−127

Owen, J.M. Pincombe, J.R. and Rogers, R.H. 1985, Source−sink flow inside a rotating cylindrical cavity. J. Fluid Mech., 155, 233−265

Owen, J.M. and Rogers, R.H. 1989, Flow and heat transfer in rotating disc systems: Vol. 1, Rotor−stator systems [Research Studies Press, Taunton, UK and John Wiley, New York, USA]

Chew, J.W., Owen, J.M. and Pincombe, J.R. 1984, Numerical predictions for laminar source−sink flow in a rotating cylindrical cavity. J. Fluid Mech., 143, 451−466

Owen, J.M. and Rogers, R.H. 1995, Flow and heat transfer in rotating disc systems: Vol. 2, Rotating cavities [Research Studies Press, Taunton, UK and John Wiley, New York, USA]

Vaughan, C. M., Gilham, S. and Chew, J. W. 1989, Numerical solutions of rotating disc flows using a non−linear multigrid algorithm. Proc. 6th Conf. Num. Meth. Lam. Turb. Flow, Swansea, 66−73 [Pineridge Press, Swansea]

Wilson, M., Pilbrow, R and Owen, J.M., 1995 Flow and heat transfer in a pre−swirl rotor−stator system. 40th ASME Int. Gas Turbine and Aeroengine Cong., Houston, June 1995. Paper 95−GT−239 (To be published in J.Turbomachinery)